UNEQUAL DIAMETERS AND THEIR EFFECTS ON TIME-VARYING VOLTAGES IN BRANCHED NEURONS

BARRY HORWITZ
Department of Mathematics and Physics, Texas Woman's University, Denton, Texas 76204

ABSTRACT A theoretical method, developed in a previous paper, enables one to calculate analytical expressions for time-varying voltages at specific locations in branching dendritic systems in response to synaptic current inputs at other sites. Exact results were obtained for a number of dendritic trees that possessed certain symmetries: all branch lengths had to be integral multiples of one another, and all branch diameters had to be equal. Because the second of these conditions is unrealistic, the method has been generalized to treat dendritic trees whose branches differ in diameter. The method entails adding onto the symmetric results a sum of correction terms. It is found that the correction terms, as well as the symmetric results, can be expressed as combinations of two families of functions. These functions, generalizations of those found in our earlier paper, provide a precise formalism for analyzing how voltage transients depend on the geometrical structure of the dendritic tree. Examples are given that show how the correction terms affect the value of the voltage, and how variations in branch diameters alter the behavior of the propagated postsynaptic potential. The implications of these results for our understanding of neuronal functioning are discussed.

INTRODUCTION

The extensive branching of the dendritic arborization imposes formidable obstacles for both experimental and theoretical studies of how neurons propagate information by means of electrotonic potentials. A key question that must be answered is the following: How is a single synaptic input at a given dendritic location "perceived" at some other neuronal site, especially a site of neural output such as a spike-generating zone? By perceived I mean what are the amplitude and time course of the voltage transient at the output position due to the injection of synaptic current at the input site? The spread of the injected current is determined by a number of parameters that can be grouped into three categories: (*a*) cable properties, the electrical parameters such as core resistance (R), membrane conductance (G), and membrane capacitance(C) that, for a given dendritic branch, can be combined to give us the space constant $\lambda = (1/RG)^{1/2}$ and the time constant $\tau = C/G$; (*b*) the synaptic parameters, the strength of the current input and its time course; (*c*) the geometrical parameters of the tree, e.g., the lengths of the branches, their respective diameters, and the number of daughter branches to a given branch.

The last of these has proved to be the most difficult to model effectively. This has been true particularly for analytical (compared with computer-compartmental) treatments. In a previous study (Horwitz, 1981 *a*), I developed a method by which the electrotonic behavior of branching dendritic systems could be studied analytically. Exact mathematical results were obtained for the transient membrane potential change at $x = 0$ due to the injection of a time-varying current at any other location in the tree for a number of model configurations (see Fig. 1). The parameter x is the anatomical (not the electrotonic) distance from the left end of the dendritic tree. These results have been used to examine how the time course and amplitude of the transient voltages were affected by changes in the geometrical parameters, especially the branching pattern distal to the synaptic input site (Horwitz, 1981 *b*). The chief assumptions placed on the geometrical parameters were that the lengths of the individual branches must be integral multiples of one another,[1] and that all branches must have the same diameter. Although the first of these does not impose serious limitations on the applicability of the model systems to elucidate neuronal behavior, the second assumption is biologically unreasonable, and therefore restricts the kind of information that can be learned. In Horwitz (1981 *a*) some brief comments were made and one example given as to how the second assumption could be eliminated. This article presents a more thorough analysis of the extension of the method to trees with unequal branch diameters.

This paper is divided into four sections. In the first, the method used in Horwitz (1981 *a*) is outlined; the second shows how we deal with trees whose branches have different diameters, while several illustrations are pre-

Dr. Horwitz's present address is the Laboratory of Neurosciences, National Institute on Aging, National Institutes of Health, Bethesda, MD.

[1] It is also possible for some of the branches to be of infinite length; these cases could model dendritic trees in which some of the branches are very long relative to others.

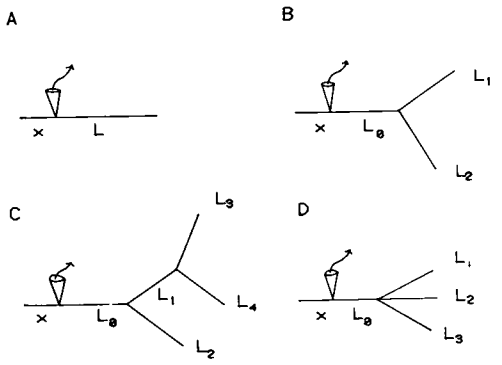

FIGURE 1 Dendritic trees whose behavior was analyzed in Horwitz (1981 *a*). In all cases the recording electrode is on the primary branch a distance x from the end ($x = 0$). (*A*) Unbranched dendritic tree of length L. (*B*) A branched dendritic tree with one primary and two secondary branches. (*C*) A branched dendritic tree with two bifurcations. (*D*) A branched dendritic tree with one primary and three secondary branches.

sented in the third; in the last section a number of issues are discussed, and some conclusions are presented. The notation used is mostly the same as in Horwitz (1981 *a*). A preliminary account of portions of this research has been reported (Horwitz, 1981 *c*).

REVIEW OF THEORETICAL METHOD

Fig. 2 is a diagram of the problem we address. Given a branched dendritic system with one synaptic input at a particular site, what is the mathematical expression for the amplitude and time course of the transmembrane potential change at some other point (denoted in the diagram by the recording electrode) due to the injection of a specified, time-dependent current $i_{sy}(t)$ at the input location? The starting point of the method is the cable differential equation for the change in the electrotonic potential, $v(x, t)$ (Rall, 1977; Jack et al., 1975):

$$\lambda^2 \frac{\partial^2 v(x,t)}{\partial x^2} - \tau \frac{\partial v(x,t)}{\partial t} - v(x,t) = 0, \qquad (1)$$

x is the physical (i.e., anatomical) position along the dendrite, t is the time. For a given branch the space and time constants are taken to be uniform.

One way to solve this partial differential equation is to employ Laplace transformation techniques (Churchill, 1958). The Laplace transform of

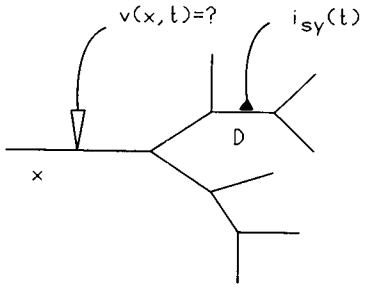

FIGURE 2 Diagram illustrating the general problem. Given a branched neuron with a synapse injecting a current $i_{sy}(t)$ into a dendritic branch a distance D from a bifurcation point, what is the time-varying voltage $v(x, t)$ at another location? The recording electrode is used to denote the position x at which the membrane potential change is to be determined.

$v(x, t)$ is defined by

$$V(x, s) = \int_0^\infty v(x, t)\, e^{-st} dt \equiv \mathcal{L}\, v(x, t). \qquad (2)$$

Eq. 1 then becomes an ordinary differential equation:

$$\frac{d^2V(x,s)}{dx^2} - \gamma^2 V(x,s) = 0 \qquad (3)$$

with

$$\gamma = \sqrt{s\tau + 1}/\lambda. \qquad (4)$$

Butz and Cowan (1974) developed a graphical calculus for generating analytical solutions for $V(x, s)$ at any point on the dendritic tree of neurons with arbitrary dendritic geometries. Using their method, one can write down the solution to Eq. 1 no matter how complicated the geometry. I showed in Horwitz (1981 *a*) how one could find the inverse Laplace transform analytically. The inverse Laplace transform is the transient voltage change, and, thus, it is the quantity of both theoretical and experimental interest. Basically, one can write any of the results of Butz and Cowan in the following form:

$$V(x, s = R(x, s)A(D, s)F(\text{Geom}, s)I_{sy}(s) \qquad (5)$$

where $R(x, s)$ is a factor that depends on the location at which the potential is to be evaluated (i.e., the recording electrode's position), $A(D, s)$ depends primarily on the position of the synaptic input, $F(\text{Geom}, s)$ depends principally on the geometry of the tree (the symbol Geom is used to denote this dependence),[2] and $I_{sy}(s)$ is the Laplace transform of the input current. Of course, each of these factors also depends on the transform parameter, s. After the inverse transform of each factor was defined by

$$r(x, t) = \mathcal{L}^{-1} R(x, s) \qquad (6)$$

$$a(D, t) = \mathcal{L}^{-1} A(D, s) \qquad (7)$$

$$f(\text{Geom}, t) = \mathcal{L}^{-1} F(\text{Geom}, s), \qquad (8)$$

the convolution theorem (Churchill, 1958) was used in Horwitz (1981 *a*) to write the transient voltage as

$$v(x, t) = \int_0^t dt_2 \int_0^{t_2} dt_3 \int_0^{t_3} dt_4 \cdot r(x, t_4) f(\text{Geom}, t_3 - t_4) a(D, t_2 - t_3) i_{sy}(t - t_2). \qquad (9)$$

$i_{sy}(t)$ incorporates the amplitude and time course of the input current. For all the cases that will be discussed in this article the input current will consist of a unit impulse of charge at $t = 0$; i.e., $i_{sy}(t) = \delta(t)$, where $\delta(t)$ is the Dirac delta function. This means that the results obtained are for the time course and amplitude of the transfer functions associated with particular synapse-recording location-geometry triads. If the synaptic current has a finite time course, one further integration of Eq. 9 is necessary. Because I shall always take the recording position to be the left end of the dendritic tree, the factor $r(x, t)$ will not change. The factors that do change as the geometry is altered are $f(\text{Geom}, t)$ and $a(D, t)$.[3]

For most dendritic trees it is not possible to provide exact mathemati-

[2] In Horwitz (1981 *a*) I denoted the geometry dependent factor by $F(G, s)$.

[3] It is also necessary to specify how each branch terminates. For most of the cases discussed in this paper each branch is assumed to terminate in a sealed end. This effectively means that the current at each terminal is zero. Other boundary conditions can be used, e.g., killed ends, lumped soma. The conclusions we reach will differ in detail, but not substance, depending on the nature of the branch terminations.

cal expressions for the input and geometry-dependent factors. However, as demonstrated in Horwitz (1981 *a*), some geometries possess certain symmetries that enable us to find these factors, and consequently to evaluate $v(t)$ exactly. I call the integral expressions for these particular trees "the primitive integrals." For a dendritic tree that deviates from the symmetric configuration,

$$v(x, t) = \text{primitive integral} + \text{correction terms.} \quad (10)$$

The trees that were analyzed in Horwitz (1981 *a*) are shown in Fig. 1. It was found that all the primitive integrals for these geometries, for any location of the synaptic input, could be expressed in terms of two closely related sets of functions, which I called the *G*-functions:

$$G_{mn;c}(L - D, t) = \frac{1}{m + n}\sum_{k=0}^{\infty} \cdot \left(\frac{m - n}{m + n}\right)^k \{g[2kL + D, t] + g[2(k + 1)L - D, t]\} \quad (11)$$

$$G_{mn;s}(L - D, t) = \frac{1}{m + n}\sum_{k=0}^{\infty} \cdot \left(\frac{m - n}{m + n}\right)^k \{g[2kL + D, t] - g[2(k + 1)L - D, t]\} \quad (12)$$

where

$$g(x, t) = \sqrt{\frac{\tau}{\pi}}\frac{x}{2\lambda t^{3/2}} e^{-t/\tau} e^{-\tau x^2/4\lambda^2 t}. \quad (13)$$

Basically, I found that for a particular configuration $a(D, t)$ and $f(\text{Geom}, t)$ would each be written as a combination of different *G*-functions; as the configuration changes, so do the particular *G*-functions in terms of which $a(D, t)$ and $f(\text{Geom}, t)$ are expressed. Much of Horwitz (1981 *a*) is is devoted to enumerating for many of the symmetric geometries associated with the trees shown in Fig. 1 the *G*-function combinations for $a(D, t)$ and $f(\text{Geom}, t)$.[4] The crucial point that emerged was that the *G*-functions provide the appropriate way to treat the behavior of these systems analytically; the *G*-functions give us a precise language for talking about the structure-function relation for dendritic trees (so long as we restrict ourselves to neurons whose branch diameters are equal).

CORRECTION TERMS FOR TREES WITH UNEQUAL DIAMETERS

If the diameters of the various branches differ, the cable parameters will not be constant throughout the tree, and thus, the corrections terms in Eq. 10 will require evaluation. To see how this is done, we begin with an example. Consider the tree shown in Fig. 1 *B*. Take the synaptic input to be located a distance D from the bifurcation on the secondary branch of length L_1.[5] The rules of Butz and Cowan (1974) give us the following expression for the Laplace transform of the potential at a point x along the primary branch:

$$V(x, s) = \frac{Z_{c_0}Z_{c_1}Z_{c_2}\cosh\gamma_0 x \cosh\gamma_2 L_2 \cosh\gamma_1(L_1 - D)}{\left[\begin{array}{l} Z_{c_0}Z_{c_1}\cosh\gamma_0 L_0 \cosh\gamma_1 L_1 \sinh\gamma_2 L_2 \\ + Z_{c_0}Z_{c_2}\cosh\gamma_0 L_0 \sinh\gamma_1 L_1 \cosh\gamma_2 L_2 \\ + Z_{c_1}Z_{c_2}\sinh\gamma_0 L_0 \cosh\gamma_1 L_1 \cosh\gamma_2 L_2 \end{array}\right]} I_{sy}(s) \quad (14)$$

where $Z_{c_i} = R_i/\gamma_i$ and $\gamma_i = (s\tau_i + 1)^{1/2}/\lambda_i$. Z_{c_i} is called the characteristic impedance of the cable. In terms of the factors in Eq. 5 we showed in Horwitz (1981 *a*) that

$$R(x, s) = Z_{c_0}\cosh\gamma_0 x. \quad (15)$$

$$A(D, s) = \frac{\cosh\gamma_1(L_1 - D)}{\cosh\gamma_1 L_1} \quad (16)$$

$$F(Geom, s) = \frac{Z_{c_1}Z_{c_2}\cosh\gamma_1 L_1 \cosh\gamma_2 L_2}{\left[\begin{array}{l} Z_{c_0}Z_{c_1}\cosh\gamma_0 L_0 \cosh\gamma_1 L_1 \sinh\gamma_2 L_2 \\ + Z_{c_0}Z_{c_2}\cosh\gamma_0 L_0 \sinh\gamma_1 L_1 \cosh\gamma_2 L_2 \\ + Z_{c_1}Z_{c_2}\sinh\gamma_0 L_0 \cosh\gamma_1 L_1 \cosh\gamma_2 L_2 \end{array}\right]} \quad (17)$$

Taking $x = 0$ allows us to write $r(0, t) = \mathcal{L}^{-1}R(0, s)$ as

$$r(0, t) = \frac{R_0\lambda_0}{\sqrt{\tau_0}}\frac{e^{-t/\tau_0}}{\sqrt{\pi t}}. \quad (18)$$

For all the cases discussed hereafter, $r(0, t)$ will always be given by Eq. 18.

In Horwitz (1981 *a*) we showed that the inverse Laplace transforms of the factors $A(D, s)$ and $F(\text{Geom}, s)$ are best written in terms of the *G*-function formalism. The key to doing this comes from relating the inverse Laplace transforms of certain combinations of hyperbolic functions to the *G*-functions; specifically,

$$G_{mn;c}(L - D, t) = \mathcal{L}^{-1}\left[\frac{\cosh\gamma(L - D)}{m\sinh\gamma L + n\cosh\gamma L}\right] \quad (19)$$

$$G_{mn;s}(L - D, t) = \mathcal{L}^{-1}\left[\frac{\sinh\gamma(L - D)}{m\sinh\gamma L + n\cosh\gamma L}\right]. \quad (20)$$

Therefore, we can invert the $A(D, s)$ of Eq. 16 quite simply:

$$a(D, t) = G_{01;c}(L_1 - D, t). \quad (21)$$

If we take all branch diameters equal, then we may equate the λ_is, Z_{c_i}s, and γ_is of each branch. $F(\text{Geom}, s)$ can then be inverted, and the resulting expression for $f(\text{Geom}, t)$ is also written in terms of the *G*-functions. The particular combination of *G*-functions that appear depends on the relative

[4] An error was made in using the Butz-Cowan (1974) rules to generate the expressions for $V(x, s)$ for the trees shown in Figs. 1 *C* and *D* of this paper (Figs. 5 and 6 of Horwitz (1981 *a*)). These expressions are found in Appendix A of Horwitz (1981 *a*). Eq. A2 should read, $\Delta_2 = \Delta_a(\cosh\gamma L_3 \sinh\gamma L_4 + \sinh\gamma L_3 \cosh\gamma L_4) + \Delta_b \cosh\gamma L_3 \cosh\gamma L_4$. Eq. A3 should read , $\Delta_a = \cosh\gamma L_0 \sinh\gamma L_1 \sinh\gamma L_2 + \cosh\gamma L_0 \cosh\gamma L_1 \cosh\gamma L_2 + \sinh\gamma L_0 \sinh\gamma L_1 \cosh\gamma L_2$. Eq. A4 should read, $\Delta_b = \sinh\gamma L_0 \cosh\gamma L_1 \cosh\gamma L_2 + \sinh\gamma L_0 \sinh\gamma L_1 \sinh\gamma L_2 + \cosh\gamma L_0 \cosh\gamma L_1 \sinh\gamma L_2$. Eq. A62 should read $\Delta_6 = \cosh\gamma L_0 \cosh\gamma L_1 \cosh\gamma L_2 \sinh\gamma L_3 + \cosh\gamma L_0 \cosh\gamma L_1 \sinh\gamma L_2 \cosh\gamma L_3 + \cosh\gamma L_0 \sinh\gamma L_1 \cosh\gamma L_2 \cosh\gamma L_3 + \sinh\gamma L_0 \cosh\gamma L_1 \cosh\gamma L_2 \cosh\gamma L_3$. Eq. A72 should read $\Delta_7 = \sinh\gamma(L_0 - D) \cosh\gamma L_1 \cosh\gamma L_2 \sinh\gamma L_3 + \sinh\gamma(L_0 - D) \cosh\gamma L_1 \sinh\gamma L_2 \cosh\gamma L_3 + \sinh\gamma(L_0 - D) \sinh\gamma L_1 \cosh\gamma L_2 \cosh\gamma L_3 + \cosh\gamma(L_0 - D) \cosh\gamma L_1 \cosh\gamma L_2 \cosh\gamma L_3$. Unfortunately, as a result of these mistakes, many of the specific expressions for $F(\text{Geom}, s)$, $f(\text{Geom}, t)$, and in some cases $A(D, s)$ and $a(D, t)$, in Appendix A are incorrect. The formulas listed here will allow a correct derivation of all the specific expressions to be made. I shall be glad to provide a corrected list of all the expressions to any reader. None of the conclusions reached in Horwitz (1981 *a*) were affected by these errors.

[5] Note that L is the physical, not the electrotonic length.

lengths of the branches. For example, if all branch lengths for the tree of Fig. 1 *B* are equal, Eq. 17 reduces to

$$F(\text{Geom}, s) = \frac{1}{3 \sinh \gamma L}, \tag{22}$$

which implies

$$f(\text{Geom}, t) = \tfrac{1}{3}\, G_{10;c}(0, t). \tag{23}$$

If $L_0 = L_2 = L$, and $L_1 = 2L$, then

$$F(\text{Geom}, s) = \frac{1}{4 \sinh \gamma L} + \frac{1}{8}\left[\frac{1}{\sinh \gamma L + i\sqrt{2} \cosh \gamma L} + \frac{1}{\sinh \gamma L - i\sqrt{2} \cosh \gamma L}\right] \tag{24}$$

which yields

$$f(\text{Geom}, t) = \tfrac{1}{4}\, G_{10;c}(0, t) + \tfrac{1}{8}\,[G_{1i\sqrt{2};c}(0, t) - G_{1-i\sqrt{2};c}(0, t)]. \tag{25}$$

A large number of examples of this sort, for the trees shown in Fig. 1, is given in Horwitz (1981 *a*).

If the branch diameters are not the same everywhere in the tree, the electrical parameters for each branch will not be equal. All three electrical parameters (membrane conductance G, core resistance R, membrane capacitance C) are functions of the diameter d of a given branch:

$$G = \frac{\pi d}{R_m} \tag{26}$$

$$R = \frac{4\rho}{\pi d^2} \tag{27}$$

$$C = \pi d C_m \tag{28}$$

where R_m is the membrane resistance of a branch unit surface area, C_m is the membrane capacitance per unit surface area, and ρ is the intracellular resistivity of the branch. The space constant λ, the quantity γ and the characteristic impedance Z_c consequently all acquire a dependence on d, although the time constant τ does not:

$$\lambda = \sqrt{\frac{R_m}{4\rho}}\, d^{1/2} \tag{29}$$

$$\gamma = \sqrt{\frac{4\rho(s\tau + 1)}{R_m}}\, d^{-1/2} \tag{30}$$

$$Z_c = \frac{R}{\gamma} = \frac{1}{\pi}\sqrt{\frac{4\rho R_m}{s\tau + 1}}\, d^{-3/2}. \tag{31}$$

Note that γ and Z_c are also functions of the transform parameter, s. Because we cannot set equal all the $\lambda_i s$, $\gamma_i s$, and $Z_{c_i} s$ in the expression for the geometry factor $F(\text{Geom}, s)$ (e.g., Eq. 17), $F(\text{Geom}, s)$ will be a function of the different branch diameters, which we can express symbolically as

$$F(\text{Geom}, s) = F(d_0, d_1, d_2, \ldots, d_n, s). \tag{32}$$

One standard approximation technique uses the Taylor expansion (in n-1 variables):

$$F(\text{Geom}, s) = F(d_0, d_0, \ldots, d_0, s) + (d_1 - d_0)\left(\frac{\partial F}{\partial d_1}\right)_{d_i = 0} + (d_2 - d_0)\left(\frac{\partial F}{\partial d_2}\right)_{d_i = d_0} + \cdots + 0\,[(d_i - d_0)^2]. \tag{33}$$

The first term on the right-hand side is the expression for the geometry factor when all the diameters are equal; i.e., it is the expression used in the primitive integral (e.g., Eq. 22 or 24).

Take each branch diameter to be some fraction of the primary branch diameter,

$$d_i = f_i d_0, \qquad i = 1, 2, \ldots, n \qquad 0 < f_i \leq 1 \tag{34}$$

and define the percentage deviations by

$$\alpha_i = 1 - f_i = -\left[\frac{d_i - d_0}{d_0}\right]. \tag{35}$$

Eq. 33 can be written in the following form:

$$F(\text{Geom}, s) = F_0 - \alpha_1 d_0 (F_1)_0 - \alpha_2 d_0 (F_2)_0 + \cdots + \tfrac{1}{2}\,[\alpha_1^2 d_0^2 (F_{11})_0 + \alpha_2^2 d_0^2 (F_{22})_0 + 2\alpha_1\alpha_2 d_0^2 (F_{12})_0 + \cdots] + 0[(d_i - d_0)^3] \tag{36}$$

where

$$F_0 = F(d_0, d_0, \ldots, d_0, s) \tag{37}$$

$$F_i = \frac{\partial F}{\partial d_i} \tag{38}$$

$$F_{ij} = \frac{\partial^2 F}{\partial d_i \partial d_j} \tag{39}$$

and thus,

$$(F_i)_0 = \left(\frac{\partial F}{\partial d_i}\right)_{d_j = d_0} \tag{40}$$

$$(F_{ij})_0 = \left(\frac{\partial^2 F}{\partial d_i \partial d_j}\right)_{d_k = d_0} \tag{41}$$

Note that in the expressions for $(F_i)_0$, $(F_{ij})_0$ and the higher-order derivatives that appear in Eq. 36 all the diameters are equal, and thus, all the $\gamma_i s$ and all the $Z_{c_i} s$ are equal to one another.

To calculate the time-varying voltage it is necessary to take the inverse Laplace transform of $F(\text{Geom}, s)$. The question arises, therefore, as to whether or not, after evaluating the derivatives in Eq. 36, the inverse transform can still be found in analytical form, and if so, can it be written in terms of the G-functions, or something similar. The answer is yes, which we now demonstrate.

Because both Z_{c_i} and γ_i are functions of d_i, we can write the first derivatives as

$$F_i = \frac{\partial F}{\partial d_i} = \frac{\partial F}{\partial \gamma_i}\frac{d\gamma_i}{dd_i} + \frac{\partial F}{\partial Z_{c_i}}\frac{dZ_{c_i}}{dd_i} = -\frac{1}{2d_i}\,[\gamma_i F_{\gamma_i} + 3Z_{c_i} F_{Z_i}] \tag{42}$$

where

$$F_{\gamma_i} = \frac{\partial F}{\partial \gamma_i} \tag{43}$$

$$F_{Z_i} = \frac{\partial F}{\partial Z_{c_i}} \tag{44}$$

Noting that

$$\frac{\partial \cosh \gamma L}{\partial \gamma} = L \sinh \gamma L \tag{45}$$

$$\frac{\partial \sinh \gamma L}{\partial \gamma} = L \cosh \gamma L \tag{46}$$

we see that F_{γ_i} (and also F_{Z_i}) will still be a rational function in the variables $\cosh\gamma_i L_i$ and $\sinh\gamma_i L_i$.

Similarly,

$$F_{ij} = \frac{1}{4d_i^2}\left\{\delta_{ij}[3\gamma_i F_{\gamma_i} + 15 Z_{c_i} F_{Z_i}] + \frac{d_i}{d_j}[\gamma_i\gamma_j F_{\gamma_i\gamma_j} + 9 Z_{c_i} Z_{c_j} F_{Z_i Z_j} + 3\gamma_i Z_{c_j} F_{\gamma_i Z_j} + 3 Z_{c_i}\gamma_j F_{Z_i\gamma_j}]\right\} \tag{47}$$

where $F_{\gamma_i\gamma_j} = \partial^2 F/\partial\gamma_i\partial\gamma_j$, etc. Analogous expressions can be written for the higher-order derivatives. It is easy to see that

$$\underbrace{F_{ijk\ldots l}}_{m \text{ indices}} \propto \underbrace{\gamma_i\gamma_j\gamma_k \cdots \gamma_l}_{m \text{ factors}} + \text{terms with } (m-1) \tag{48}$$

and fewer factors of γ_i, γ_j, etc. Therefore,

$$(F_{ijk\ldots l})_0 \propto \gamma^m + \text{terms with } \gamma^{m-1}, \gamma^{m-2}, \text{ etc.,} \tag{49}$$

because when we set the branch diameters equal, we set all the γ_is equal to γ (and all the Z_{c_i}s equal to Z_c). Hence, an alternative way to write Eq. 36 is by inserting Eqs. 42, 47, and 49 into Eq. 36, and grouping the terms together into a power series in γ:

$$F(\text{Geom}, s) = F_0\{\tilde{\phi}_0(s) + \gamma\tilde{\phi}_1(s) + \gamma^2\tilde{\phi}_2(s) + \ldots\} \tag{50}$$

where $\tilde{\phi}_i(s)$ is a rational function in the variables $\cosh\gamma L_k$ and $\sinh\gamma L_k$. Of course, each $\tilde{\phi}_i(s)$ will contain terms to all orders in the percentage deviations, α_j. It is crucial to note, however, that if we stop at the nth order correction terms (i.e., keep terms only up to the nth power in α), then the infinite series in Eq. 50 terminates with $\gamma^n\tilde{\phi}_n(s)$.

Restricting our attention to the cases in which the ratios of the dendritic lengths can be written as the ratios of integers, the multiple-angle formulae can be used so that, ultimately, we can express $\tilde{\phi}_i(s)$ in the form N/D, where both N and D are polynomials in the variables $\cosh\gamma L$ and $\sinh\gamma L$, L being a particular length. As shown in Horwitz (1981 *a*, pp. 177–178), this means that $\tilde{\phi}_i(s)$ can be inverted and written as a convolution product of the G-functions.

Recall that γ is a function of the transform parameter. Therefore, to find $f(\text{Geom}, t) = \mathcal{L}^{-1}F(\text{Geom}, s)$ we must be able to find $\mathcal{L}^{-1}[\gamma^j\tilde{\phi}_j(s)]$. In the worst possible situation we need to be able to determine what I will henceforth call "the generalized G-functions":

$$G^{(j)}_{mn;c}(L-D, t) = \mathcal{L}^{-1}\left\{\frac{\gamma^j \cosh\gamma(L-D)}{m\sinh\gamma L + n\cosh\gamma L}\right\} \tag{51}$$

$$G^{(j)}_{mn;s}(L-D, t) = \mathcal{L}^{-1}\left\{\frac{\gamma^j \sinh\gamma(L-D)}{m\sinh\gamma L + n\cosh\gamma L}\right\}. \tag{52}$$

Obviously, by assigning names to the inverse transforms I am implying that one can indeed find analytical forms for them. The procedure is quite similar to that used in Horwitz (1981 *a*) to arrive at the G-functions. There I showed that

$$\frac{\cosh\gamma(L-D)}{m\sinh\gamma L + n\cosh\gamma L} = \frac{1}{m+n}\sum_{k=0}^{\infty}\left(\frac{m-n}{m+n}\right)^k \cdot \{e^{-\gamma(2kL+D)} + e^{-\gamma[2(k+1)L-D]}\}. \tag{53}$$

We now define the generalized g-functions by

$$g_j(x, t) = \sqrt{\frac{\tau^j}{2^{j+1}\pi}}\frac{e^{-t/\tau}e^{-\tau x^2/8\lambda^2 t}}{\lambda^j t^{1+j/2}} D_{j+1}\left(\frac{x}{\lambda}\sqrt{\frac{\tau}{2t}}\right), \quad j = 0, 1, 2, \ldots \tag{54}$$

where $D_k(z)$ is the parabolic cylinder function (Magnus et al., 1966). Use of $\mathcal{L}^{-1}[\gamma^j\exp(-\gamma x)] = g_j(x, t)$ (Oberhettinger and Badii, 1973) allows us to write

$$G^{(j)}_{mn;c}(L-D, t) = \frac{1}{m+n}\sum_{k=0}^{\infty}\left(\frac{m-n}{m+n}\right)^k \cdot \{g_j[2kL + D, t] + g_j[2(k+1)L - D, t]\}, \quad j = 0, 1, 2, \ldots \tag{55}$$

Similarly,

$$G^{(j)}_{mn;s}(L-D, t) = \frac{1}{m+n}\sum_{k=0}^{\infty}\left(\frac{m-n}{m+n}\right)^k \cdot \{g_j[2kL + D, t] - g_j[2(k+1)L - D, t]\} \quad j = 0, 1, 2, \ldots \tag{56}$$

The significance of these results is the following: All the correction terms, to all orders of approximation, can be expressed in terms of a convolution product of generalized G-functions. Because the nth order term of Eq. 36 contains γ to a maximum power n, it follows that the nth order correction term to $f(\text{Geom}, t)$ can be written (in the worst possible case, where no simplifications can be made) in terms of $G^{(n)}$, $G^{(n-1)}$, ... $G^{(0)}$.

Before giving some examples in which the correction terms are evaluated, let us briefly look at a few properties of the generalized G-functions. We first consider the generalized g-functions. Listing the first few is instructive:[6]

$$g_0(x, t) = \frac{\sqrt{\tau}\,x}{2\sqrt{\pi}\,\lambda t^{3/2}} e^{-t/\tau}e^{-\tau x^2/4\lambda^2 t} \tag{57}$$

$$g_1(x, t) = \frac{1}{2\lambda}\sqrt{\frac{\tau}{\pi}}\left(\frac{\tau}{2t}\frac{x^2}{\lambda^2} - 1\right)\frac{1}{t^{3/2}} e^{-t/\tau}e^{-\tau x^2/4\lambda^2 t} \tag{58}$$

$$= \frac{1}{\lambda}\left(\frac{\tau}{\lambda}\frac{x}{2t} - \frac{\lambda}{x}\right) g_0(x, t) \tag{59}$$

$$g_2(x, t) = \frac{\tau}{2\lambda^2 t}\left(\frac{x^2}{\lambda^2}\frac{\tau}{2t} - 3\right) g_0(x, t). \tag{60}$$

Three points of importance emerge. First, comparing Eqs. 13 and 57 shows that the original g-function, the g-function used in Horwitz

[6]From Magnus et al. (1966) $D_0(z) = \exp(-z^2/4)$, $D_1(z) = z\exp(-z^2/4)$, $D_2(z) = (z^2-1)\exp(-z^2/4)$, and $D_3(z) = (z^3-3z)\exp(-z^2/4)$.

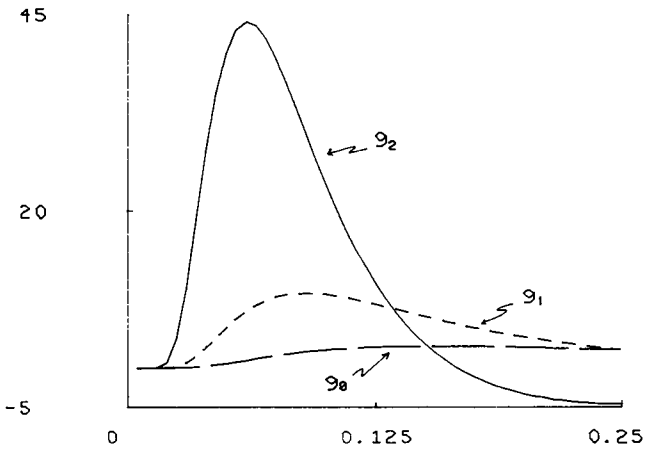

FIGURE 3 Plots of $g_j(x, t)$ vs. t/τ. Shown are g_0, g_1, and g_2 for $x/\lambda = 1$. Note that the time is expressed in terms of the time constant. The units were chosen such that $\tau = (2\sqrt{\pi})^{-1}$.

(1981 *a*), is a special case of the generalized *g*-function: it is the generalized *g*-function of zero order.[7]

Second, if we use the fact that parabolic cylinder functions obey the recurrence relation (Magnus et al., 1966)

$$D_{n+1}(z) = z\, D_n(z) - n\, D_{n-1}(z) \tag{61}$$

we can obtain a recurrence relation for the generalized *g*-functions:

$$g_{n+1}(x, t) = \frac{\tau}{2t}\frac{x}{\lambda^2} g_n(x, t) - \frac{\tau}{2t}\frac{(n+1)}{\lambda^2} g_{n-1}(x, t). \tag{62}$$

Noting from Eq. 59 that $g_1(x, t)$ can be written in terms of $g_0(x, t)$, the recurrence relation allows us, therefore, to express all the higher-order generalized *g*-functions in terms of the one of lowest order, $g_0(x, t)$. Eq. 60 is an example.

The third significant point arises by looking at the derivative of $g_0(x, t)$ with respect to x:

$$\frac{\partial g_0(x, t)}{\partial x} = \left(\frac{1}{x} - \frac{\tau x}{2\lambda^2 t}\right) g_0(x, t). \tag{63}$$

Thus,

$$g_1(x, t) = -\frac{\partial g_0(x, t)}{\partial x}. \tag{64}$$

Similarly, we can show

$$g_2(x, t) = -\frac{\partial g_1(x, t)}{\partial x} = \frac{\partial^2 g_0(x, t)}{\partial x^2}. \tag{65}$$

Indeed, using the recurrence relation, Eq. (62), one can prove by induction that

$$g_n(x, t) = -\frac{\partial g_{n-1}(x, t)}{\partial x} = (-1)^n \frac{\partial^n g_0(x, t)}{\partial x^n}. \tag{66}$$

Consequently, another way to obtain the higher-order generalized *g* functions is to start with $g_0(x, t)$ and differentiate with respect to x.

[7]Of course, this had to be so, because $g_n(x, t) \equiv \mathcal{L}^{-1}(\gamma^n e^{-\gamma x})$ and $g(x, t) \equiv \mathcal{L}^{-1}(e^{-\gamma x})$.

Fig. 3 shows graphs of the time behavior of several of the lower-order generalized *g* functions.

Turning now to the generalized *G*-functions, we see that because $g_0(x, t)$ is the *g*-function of Horwitz (1981 *a*), it follows that $G^{(0)}$, the generalized *G*-function of order zero, is the *G*-function that likewise was used in Horwitz (1981 *a*). In Fig. 4 I illustrate the behavior in time of several of the generalized *G*-functions of low order.

We now illustrate this formalism with two examples. The first is the one with which we began this section: a tree with one primary and two secondary branches (Fig. 1 *B*); the synapse is located a distance D from the bifurcation on the secondary branch of length L_1. The expression for $F(\text{Geom}, s)$ is given by Eq. 17. For cases like this, where there is a symmetry, simplifications are possible. Specifically, suppose branches i and j possess the same relationship to the tree (e.g., both branches are terminal secondary branches, or both are terminal tertiary branches, etc.). Then

$$F(i, j, s) = F(j, i, s) \tag{67}$$

where the above equation means that $F(\text{Geom}, s)$ is invariant with respect to an interchange in all the variables associated with branches i and j (i.e., $Z_{c_i} \rightleftharpoons Z_{c_j}$, $\gamma_i \rightleftharpoons \gamma_j$, $L_i \rightleftharpoons L_j$). This implies that $F(\text{Geom}, s)$ is invariant with respect to exchanging L_i and d_i with L_j and d_j.

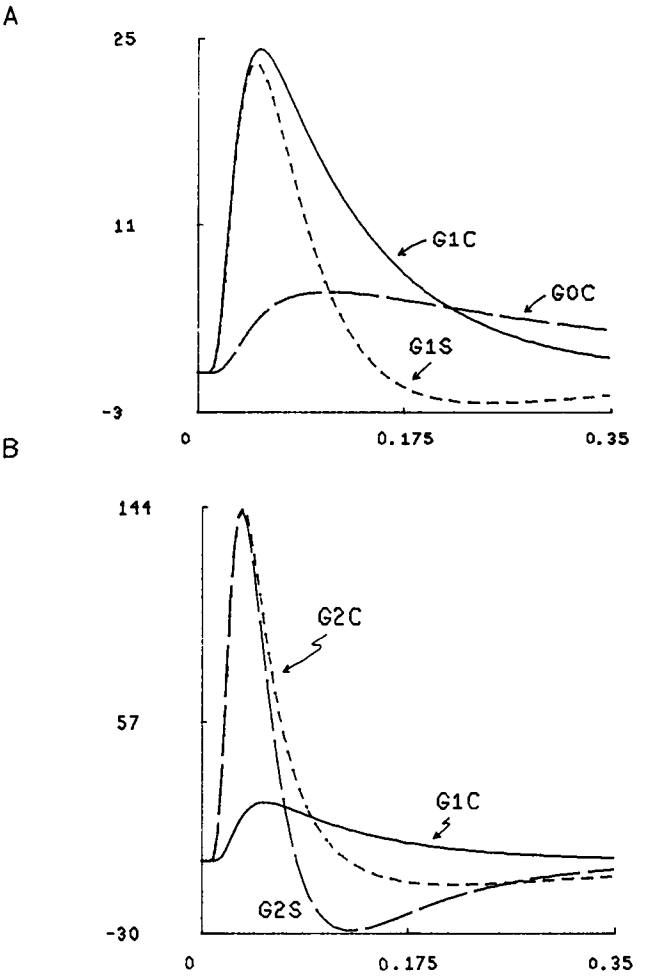

FIGURE 4 Plots of $G^{(j)}_{10,c}(L - D, t)$ and $G^{(j)}_{10,s}(L - D, t)$ vs. t/τ. (*A*) Plotted are $G^{(0)}_{10,c}(L - D, t)$ [G0C], $G^{(1)}_{10,c}(L - D, t)$ [G1C] and $G^{(1)}_{10,s}(L - D, t)$ [G1S]. (*B*) Plotted are $G^{(1)}_{10,c}(L - D, t)$ [G1C], $G^{(2)}_{10,c}(L - D, t)$ [G2C] and $G^{(2)}_{10,s}(L - D, t)$ [G2S]. For both *A* and *B* we chose $L = \lambda$, $D = 0.75\,\lambda$. The units for the time axis are the same as in Fig. 3.

Hence, for this situation[8]

$$F_i = \frac{\partial F}{\partial d_i} = F_j = \frac{\partial F}{\partial d_j} = \frac{1}{2}\frac{\partial F}{\partial d} \equiv \frac{1}{2}F' \tag{68}$$

where $\partial F/\partial d$ is obtained by setting $d_i = d_j$ in the expression for F and then differentiating. Similarly,

$$F_{ij} = \frac{\partial^2 F}{\partial d_i \partial d_j} = F_{ji} = \frac{1}{4}\frac{\partial^2 F}{\partial d^2} \equiv \frac{1}{4}F''. \tag{69}$$

Consequently, Eq. 36 can be written

$$F(\text{Geom}, s) = F_0 - \alpha_{12} d_0 F_0' + \tfrac{1}{2}\alpha_{12}^2 d_0^2 F_0'' + 0(\alpha_{12}^3) \tag{70}$$

with

$$\alpha_{12} = -\frac{1}{2d_0}(d_1 + d_2 - 2d_0) = \tfrac{1}{2}(2 - f_1 - f_2). \tag{71}$$

We now consider the specific geometry for which $L_0 = L_1 = L_2 \equiv L$. We find

$$F_0 = \frac{1}{3\sinh \gamma L} \tag{72}$$

$$F_0' = -\frac{F_0}{d_0}\left[1 + \frac{\gamma L}{3}\left(\frac{\sinh \gamma L}{\cosh \gamma L} - \frac{\cosh \gamma L}{\sinh \gamma L}\right)\right] \tag{73}$$

$$F_0'' = \frac{3F_0}{4d_0^2}\left[2 + \frac{10\gamma L}{9}\left(\frac{\sinh \gamma L}{\cosh \gamma L} - \frac{\cosh \gamma L}{\sinh \gamma L}\right) + \frac{4}{27}(\gamma L)^2\left(\frac{1}{\cosh^2 \gamma L} + \frac{2}{\sinh^2 \gamma L}\right)\right] \tag{74}$$

and, as a result, Eq. 70 becomes

$$F(\text{Geom}, s) = F_0\left[(1 + \alpha_{12} + \frac{3}{4}\alpha_{12}^2) + \frac{\gamma L}{3}\left(\alpha_{12} + \frac{5}{4}\alpha_{12}^2\right)\left(\frac{\sinh \gamma L}{\cosh \gamma L} - \frac{\cosh \gamma L}{\sinh \gamma L}\right) + \frac{(\gamma L)^2}{18}\alpha_{12}^2\left(\frac{1}{\cosh^2 \gamma L} + \frac{2}{\sinh^2 \gamma L}\right)\right] + 0(\alpha_{12}^3). \tag{75}$$

The inverse transform can now be obtained:

$$f(\text{Geom}, t) = \frac{1}{3}G_{10;c}^{(0)}(0, t) * \left\{(1 + \alpha_{12} + \frac{3}{4}\alpha_{12}^2)\delta(t) + (\alpha_{12} + \frac{5}{4}\alpha_{12}^2)\frac{L}{3}(G_{01;s}^{(1)}(L, t) - G_{10;c}^{(1)}(L, t) + \frac{L^2\alpha_{12}^2}{18} \cdot [G_{01;c}^{(1)}(0, t) * G_{01;c}^{(1)}(0, t) + 2G_{10;c}^{(1)}(0, t) * G_{10;c}^{(1)}(0, t)]\right\} + 0(\alpha_{12}^3) \tag{76}$$

where the asterisk (*) in Eq. (76) means convolution, i.e.,

$$m(t) * n(t) = \int_0^t m(t')n(t - t')\mathrm{d}t'. \tag{77}$$

Inserting Eqs. 18, 21, and 76 into Eq. 9 and then numerically performing the integrations gives us, to second order, the time-varying voltage at $x = 0$. The results of this evaluation are discussed in the next section.

As a second example, we consider the same tree, but with the synapse located a distance D from $x = 0$ on the primary branch. For this configuration (see Horwitz, 1981 *a*)

$$V(0, s) = Z_{c_0}\frac{\Delta_N}{\Delta_1}I_{sy}(s) \tag{78}$$

where

$$\Delta_N = Z_{c_0}Z_{c_1}\sinh \gamma_0(L_0 - D)\cosh \gamma_1 L_1 \sinh \gamma_2 L_2 + Z_{c_0}Z_{c_2}\sinh \gamma_0(L_0 - D)\sinh \gamma_1 L_1 \cosh \gamma_2 L_2 + Z_{c_1}Z_{c_2}\cosh \gamma_0(L_0 - D)\cosh \gamma_1 L_1 \cosh \gamma_2 L_2 \tag{79}$$

and

$$\Delta_1 = Z_{c_0}Z_{c_1}\cosh \gamma_0 L_0 \cosh \gamma_1 L_1 \sinh \gamma_2 L_2 + Z_{c_0}Z_{c_2}\cosh \gamma_0 L_0 \sinh \gamma_1 L_1 \cosh \gamma_2 L_2 + Z_{c_1}Z_{c_2}\sinh \gamma_0 L_0 \cosh \gamma_1 L_1 \cosh \gamma_2 L_2. \tag{80}$$

We chose

$$F(\text{Geom}, s) = 1 \tag{81}$$

$$A(D, s) = \frac{\Delta_N}{\Delta_1}. \tag{82}$$

As before, $r(0, t)$ is given by Eq. 18; $f(G, t) = \delta(t)$. Consequently, the approximation procedure must be applied to $A(D, s)$. The same equations hold as in the previous case (e.g., Eqs. 36, 42, 47, and 70), except A replaces F. Let us consider the specific geometry where $L_0 = L_1 = L_2 \equiv L$. Because the invariance expressed by Eq. 67 is applicable to this situation, we use the expansion given by the analogue to Eq. 70:

$$A(D, s) = A_0 - \alpha_{12} d_0 A_0' + \tfrac{1}{2}\alpha_{12}^2 d_0^2 A_0'' + 0(\alpha_{12}^3) \tag{83}$$

with α_{12} being defined by Eq. 71. We find

$$A_0 = \frac{2}{3}\frac{\sinh \gamma(L - D)}{\cosh \gamma L} + \frac{1}{3}\frac{\cosh \gamma(L - D)}{\sinh \gamma L} \tag{84}$$

$$A_0' = \frac{1}{9d_0}\left[\frac{\sinh \gamma(L - D)}{\cosh \gamma L} - \frac{\cosh \gamma(L - D)}{\sinh \gamma L}\right] \cdot \left[3 - \gamma L\left(\frac{\cosh \gamma L}{\sinh \gamma L} - \frac{\sinh \gamma L}{\cosh \gamma L}\right)\right] \tag{85}$$

$$A_0'' = \frac{-1}{2d_0^2}\left[\frac{\sinh \gamma(L - D)}{\cosh \gamma L} - \frac{\cosh \gamma(L - D)}{\sinh \gamma L}\right] \cdot \left[1 - \left(\frac{5\gamma L}{9}\frac{\cosh \gamma L}{\sinh \gamma L} - \frac{\sinh \gamma L}{\cosh \gamma L}\right) - \frac{2\gamma^2 L^2}{27}\left(3 - \frac{4}{\cosh^2 \gamma L} - \frac{2}{\text{sihn}^2 \gamma L} - \frac{3\sinh^2 \gamma L}{\cosh^2 \gamma L}\right)\right]. \tag{86}$$

[8] We have assumed in Eq. 68 two symmetric branches; if we have N symmetric branches, $F_i = F'/N$.

Thus,

$$A(D,s) = \left[\frac{2}{3}\frac{\sinh\gamma(L-D)}{\cosh\gamma L} + \frac{1}{3}\frac{\cosh\gamma(L-D)}{\sinh\gamma L}\right] + \left[\frac{\sinh\gamma(L-D)}{\cosh\gamma L} - \frac{\cosh\gamma(L-D)}{\sinh\gamma L}\right] \cdot \left[-\frac{\alpha_{12}}{3} - \frac{\alpha_{12}^2}{4} + \gamma L\left(\frac{\alpha_{12}}{9} + \frac{5\alpha_{12}^2}{36}\right) \cdot \left(\frac{\cosh\gamma L}{\sinh\gamma L} - \frac{\sinh\gamma L}{\cosh\gamma L}\right) + \frac{(\gamma L)^2}{54}\alpha_{12}^2 \cdot \left(3 - \frac{4}{\cosh^2\gamma L} - \frac{2}{\sinh^2\gamma L} - \frac{3\sinh^2\gamma L}{\cosh^2\gamma L}\right)\right]. \quad (87)$$

Taking the inverse Laplace transform gives us

$$a(D,t) = \frac{2}{3}G^{(0)}_{01;s}(L-D,t) + \frac{1}{3}G^{(0)}_{10;c}(L-D,t) + [G^{(0)}_{01;s}(L-D,t) - G^{(0)}_{10;c}(L-D,t)] * \left\{-\left(\frac{\alpha_{12}}{3} + \frac{\alpha_{12}^2}{4}\right)\delta(t) + L\left(\frac{\alpha_{12}}{9} + \frac{5\alpha_{12}^2}{36}\right)[G^{(1)}_{10;c}(L,t) - G^{(1)}_{01;s}(L,t)] + \frac{L^2\alpha_{12}^2}{54}[3\delta^{(2)}(t) - 4G^{(1)}_{01;c}(0,t) * G^{(1)}_{01;c}(0,t) - 2G^{(1)}_{10;c}(0,t) * G^{(1)}_{10;c}(0,t) - 3G^{(1)}_{01;s}(L,t) * G^{(1)}_{01;s}(L,t)]\right\} \quad (88)$$

where the following definition is used:

$$G^{(0)} * \delta^{(2)}(t) \equiv G^{(2)}. \quad (89)$$

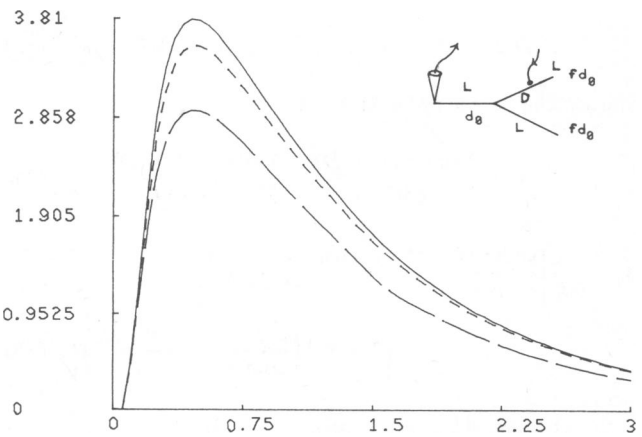

FIGURE 5 A plot of $v(0,t)$ vs. t/τ for the geometry shown in the *inset*. The three branches have equal lengths $L = \lambda_0$. The synapse is on a secondary branch a distance $D = 0.25\,\lambda_0$ from the bifurcation. Each peripheral branch diameter equals 63% of the main branch diameter ($f = 0.63$). Shown are $v(0,t)$ with the zeroth-(long dashes), first-(short dashes), and second-order (solid line) correction terms retained. The units are such that $\tau = (2\sqrt{\pi})^{-1}$, $R\lambda_0 = 3\sqrt{\pi}$, and $Q = 1$.

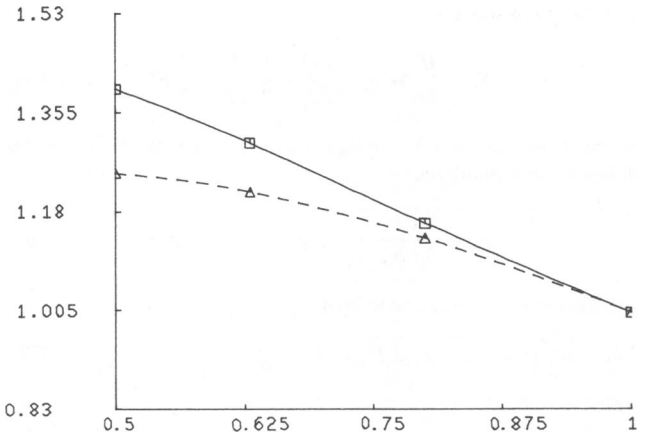

FIGURE 6 A plot of the percentage change in the peak voltage (v_m) as a function of f, the fractional change in the peripheral diameter, for the tree shown in Fig. 5. The dashed curve shows the percentage change when only first-order corrections are kept, while the solid curve shows the change when both first- and second-order terms are included. The points indicated by the triangles (△) (first order) and by the squares (□) (second order) correspond to the specific values $f = 0.5, 0.63, 0.80, 1.0$. $L = \lambda_0$. $D = 0.25\,\lambda$.

Although the algebra can become tedious, other geometries can be treated in a similar fashion. Moreover, the higher-order correction terms can also be determined, if they are needed.

NUMERICAL EXAMPLE

In this section the results of numerically evaluating the time-varying voltage for a specific configuration will be presented. Three purposes will be served in doing this. First, we shall see how the correction terms of different orders affect the value of the voltage. Second, we shall compare our approximate results with an exact evaluation of $v(0,t)$, thus determining how good the approximation technique is. Finally, we shall examine how variations in branch diameters alter the amplitude and time course of the propagated postsynaptic potential.

As the specific illustration, we take the first example of the previous section: the dendritic tree shown in Fig. 1 *B*, with all branch lengths equal to L; the synapse, which injects an impulse of unit charge at $t = 0$, is on a secondary branch a distance D from the bifurcation. Eqs. 18, 21, and 76 are inserted into the expression for the voltage at $x = 0$, Eq. 9, and the resulting integrations are performed numerically.[9]

A typical plot for $v(0,t)$ vs. t is shown in Fig. 5. For this case the synapse is a distance $D = L/4$ from the bifurcation. Each secondary branch has a diameter that is 63% of the primary branch diameter. The length of each branch was chosen to be λ_0, the value of the space constant for the primary branch. The three graphs show the results when no correction terms are kept (zeroth order), and when first- and second-order terms are included in the calculation.

[9]The methods used to do these integrations are the same as in Horwitz (1981 *a*).

The units chosen were the same as in Horwitz (1981 *a*); i.e., $\tau = (2\sqrt{\pi})^{-1}$, $R\lambda = 3\sqrt{\pi}$, $Q = 1$. As can be seen, both the amplitude and the half-width (the width of the curve at half of maximum amplitude) increase as higher-order terms are included. The percentage change depends on the diameters of the secondary branches,[10] as is shown in Fig. 6 where the percentage change in the peak amplitude is plotted as a function of f (recall $d_1 = d_2 = fd_0$). One sees that, as expected, when f is near one, the correction terms add very little, but as the peripheral branches become thinner, the correction terms become increasingly more significant.[11]

How good is our approximation? Must we include third-order terms and higher? There is one value of the fraction f for which we can compare our results with an exact evaluation of $v(0, t)$. Rall (1962 *a*) showed that when the diameters of the daughter branches were related to that of the parent branch by the 3/2 rule

$$d_0^{3/2} = \sum_{i=1}^{N} d_j^{3/2} \tag{90}$$

then the entire tree could be represented by a single cable (the equivalent cylinder model). For our geometry this case corresponds to the choice $f = 0.63$. Fig. 7 shows the results of such a comparison. In Fig. 7 *A* we plot the peak amplitude v_m as a function of synaptic location D. The solid curve corresponds to the use of Eq. 76 with $f = 0.63$, and keeping terms up to second order; the triangles (Δ) are the values of v_m obtained by the use of the equivalent cylinder, and hence represent the exact values of v_m. Fig. 7 *B* shows the analogous results for half-width ($\Delta T_{1/2}$) vs. D. As can be seen, the agreement is quite good. Therefore, the conclusion is that, at least for the geometry shown in Fig. 1 *B*, for $f \geq 0.63$, the method used in this paper, keeping approximation terms no higher than second order gives transient voltage values that are within a few percent of the ones that would have been obtained if the calculation had been done exactly. I suspect that for $0.5 \leq f < 0.63$, the second-order results would be within 10% of the exact values. It would be unusual for both daughter branches to have $f < 0.5$.

It is important to note that it is not f, but $\alpha_{12} = (2 - f_1 - f_2)/2$, that is the approximation parameter. Thus, what we want for good results is not $f \geq 0.5$, but $\alpha_{12} \leq 0.5$. This means that our model can treat the situation where a dendrite bifurcates into two branches of unequal diameters, even the case where a branch gives off a thin collateral. Indeed, as can be seen from Eq. 70, once we have evaluated the derivatives [e.g., $(F_i)_0$, $(F_{ij})_0$], all possible combinations of f_1 and f_2 can be considered, and so long as $\alpha_{12} \leq 0.5$, we can expect excellent results.

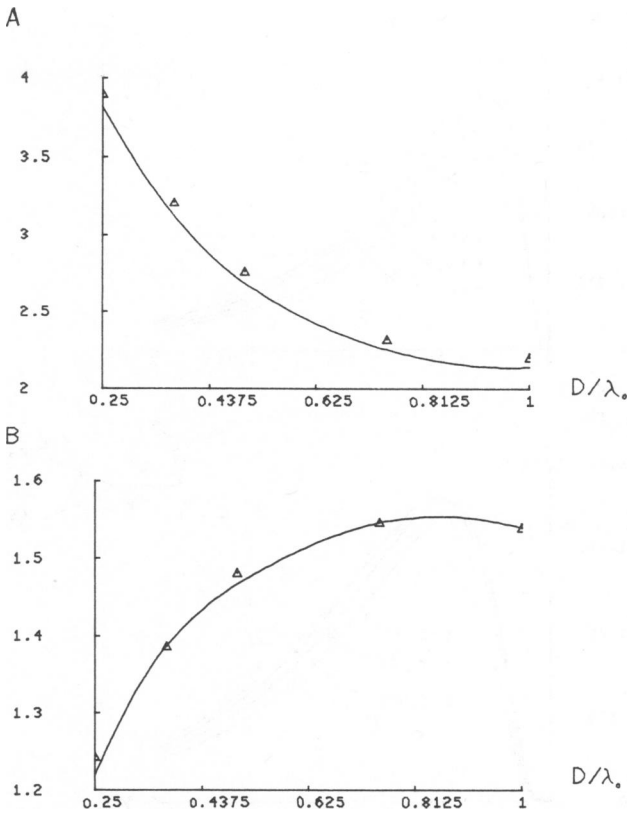

FIGURE 7 (*A*) A plot of peak amplitude (v_m) vs. synaptic location D. (*B*) A plot of half-width ($\Delta T_{1/2}$) vs. synaptic location D. For both, the solid curve corresponds to the use of Eq. 76 with $f = 0.63$, and keeping terms up to second order; the triangles (Δ) are the values of v_m (or $\Delta T_{1/2}$) obtained by use of the equivalent cylinder. They represent the exact values of v_m (or $\Delta T_{1/2}$). Synaptic location is expressed in units of the space constant λ_0; half-width is in units of the time constant τ. All other units are the same as in Fig. 5.

We conclude this section by illustrating how variations in branch diameters affect the way a postsynaptic potential (PSP) is perceived at some downstream point in the neuron. We continue with the configuration illustrated above (in which $L_0 = L_1 = L_2 \equiv L$, and $d_1 = f_1 d_0$, $d_2 = f_2 d_0$). Fig. 8 shows the time behavior of $v(0, t)$ for various values of $f_1 = f_2 = f$. For Fig. 8 *A* the synaptic location, D, is $L/4$ from the bifurcation point, whereas $D = 3L/4$ for the graphs shown in Fig. 8 *B*. We have included correction terms up to second order in α_{12}.[12] Note that both the time course and the amplitude of the potential observed at $x = 0$ are affected by the changes in branch diameters.

[10]It also depends on the location of the synapse and the lengths of the branches. A detailed study of these dependencies will be presented elsewhere.

[11]Note that the first-order corrections are not linear in f, and the second-order corrections are not quadratic. The correction terms for f(Geom, t) are linear and quadratic, respectively, but the parameter f also enters in the expression for $a(D, t)$; $a(D, t)$ is written in terms of the g-functions of order zero, and the space constant appears in the definition of g_0. On a peripheral branch, $\lambda = \lambda_0/\sqrt{f}$, where λ_0 is the value of the space constant on the primary branch.

[12]Fig. 12 of Horwitz (1981 *a*) represents the same arrangement as does Fig. 8 *A*, except there our results included only first-order correction terms.

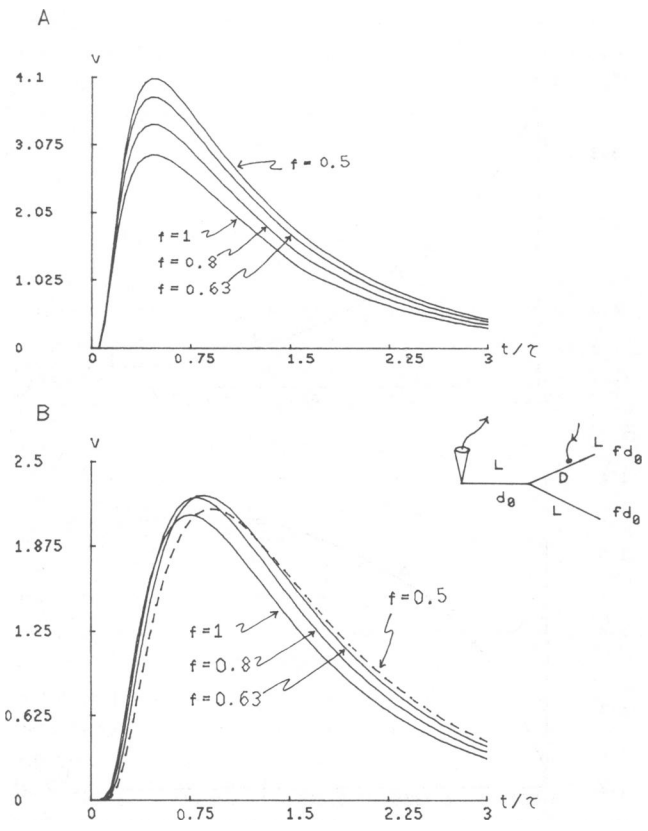

FIGURE 8 Plots of $v(0, t)$ vs. t/τ for the geometry shown in the *inset* (same as for Fig. 5). All three branches have length equal to that of the space constant for the primary branch (λ_0). Each peripheral branch has diameter equal to fd_0, where d_0 is the primary branch diameter. In *A* the synaptic input is on the secondary branch a distance $L/4$ from the bifurcation, $L = \lambda_0$, $D = 0.25\,\lambda_0$; in *B* the synaptic input is $3L/4$ from the junction, $L = \lambda_0$, and $D = 0.75\,\lambda_0$. The units are the same as in Fig. 5. The calculations were done keeping terms up to second order.

The size and shape of the v vs. t curve reflects the way in which the core resistance, the membrane resistance, and the membrane capacitance are dependent upon the geometry of the tree. When synaptic current enters a tree, some will flow distally, some will pass into side branches, and some will pass to $x = 0$ where it results in a voltage change. As the membrane capacitance becomes discharged, a process that takes time, some of the propagating current will exit through the membrane resistances. Thus, at any given time the amount flowing toward $x = 0$ depends on the relative impedances of all the other current paths; as time proceeds, these change because of the discharging membrane capacitors. Increasing the length of a branch increases the total core resistance, the total membrane capacitance, but decreases the total membrane resistance (i.e., we now have more membrane resistors in parallel). Increasing the branch diameter lowers the first and third of these, but it increases the second.

For example, looking at Fig. 8 *A* we see that as the diameter decreases, the current drawn toward the periphery, both in the branch into which the current is injected and in the other side branch, gets small; more current is thus received at $x = 0$, resulting in a larger recorded voltage change. However, when the position of the input site is more distally located, as is the situation pictured in Fig. 8 *B*, the balance between the centrifugal and centripetal currents is different (recall that the current must be zero at the sealed end terminations). Now a thin branch results in much greater attenuation of the centripetal current. Indeed, as Fig. 8 *B* demonstrates, when $f = 0.5$, we have a smaller peak voltage than when $f > 0.63$.

Fig. 9 shows what happens when the two secondary branch diameters are unequal. For Fig. 9 *A* the branch on which the synapse is located has the same diameter as the primary branch. The four graphs, showing the voltage at $x = 0$, correspond to letting the other secondary branch diameter change from being the same as the primary branch ($f_2 = 1$) to being very thin ($f_2 = 0.5$). In Fig. 9 *B* the geometry is reversed: the branch on which the synapse resides changes diameter, while the other secondary branch diameter remains equal to that of the primary

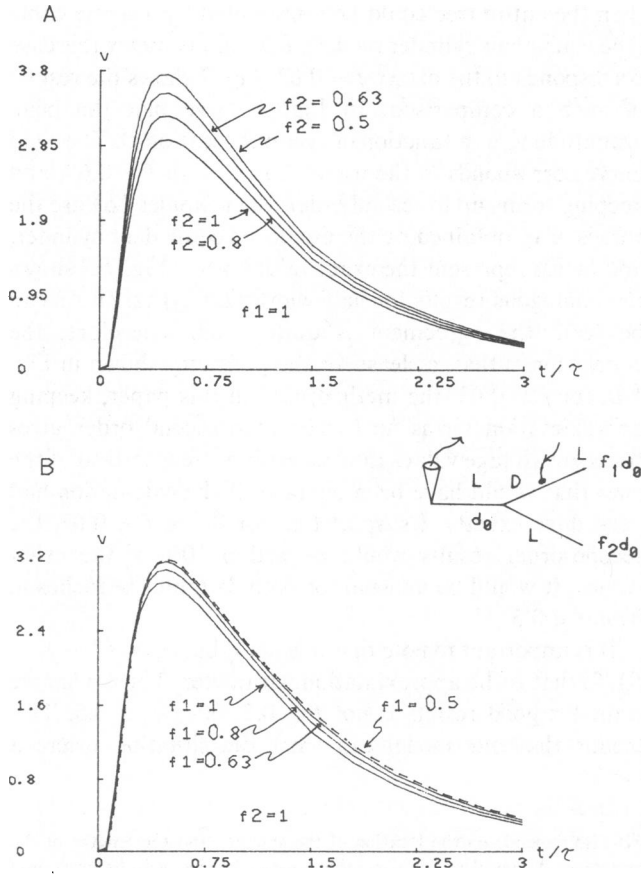

FIGURE 9 Plots of $v(0, t)$ vs. t/τ for the geometry shown in the *inset*. As for Fig. 8, all three branches have the same length ($L = \lambda_0$). The diameters of the peripheral branches are $d_1 = f_1 d_0$, $d_2 = f_2 d_0$, where d_0 is the diameter of the primary branch. The synaptic input is located on branch 1 a distance $D = 0.25L$ from the bifurcation. The units are the same as in Fig. 5. In *A* $f_1 = 1$ and we plot $v(0, t)$ for $f_2 = 1$, 0.8, 0.63, and 0.5. In *B* $f_2 = 1$, and graphs for $f_1 = 1$, 0.8, 0.63, and 0.5 are shown. The calculations kept terms up to second order.

TABLE I
PERCENTAGE CHANGE IN PEAK VOLTAGE
(FROM FIGS. 8*A*, 9*A*, 9*B*)

	$f = 1$	$f = 0.8$	$f = 0.63$	$f = 0.5$
	%	%	%	%
$f = 1$	0	10	20	28
$f = 0.8$	5	16		
$f = 0.63$	7.5		30	
$f = 0.5$	8			40

branch. For both cases the synapse is a distance $L/4$ from the bifurcation.

Besides examining the two sets of graphs, added insight can be gained by including Fig. 8 *A* in the analysis. A quantitative summary is presented in Table I, in which the percentage change in the value of the peak voltage, compared with the tree in which all diameters are equal ($f_1 = f_2 = 1$), is listed for each configuration. To illustrate, compare the case where $f_1 = 1, f_2 = 0.63$ (Fig. 9 *A*) with that for which $f_1 = 0.63, f_2 = 1$ (Fig. 9 *B*), and compare both with the tree in which $f_1 = f_2 = 0.63$ (Fig. 8 *A*). The percentage changes in the peak voltages are 20, 7.5, and 30%, respectively.[13] Because similar behavior is seen for all the other configurations, we conclude that for this specific tree, with the synapse, in particular, located near the bifurcation, the peak voltage at $x = 0$ is influenced primarily by how much of the injected current flows into the other secondary branch. The thinner it becomes, the more resistance it presents, and consequently, more of the current flows toward $x = 0$, resulting in a larger peak voltage change.

This example shows the value of the method. The precise way in which geometry affects the propagation of a postsynaptic potential can be studied. One can determine in a systematic fashion how changes in dendritic length, dendritic diameter, and in branching both proximal and distal to a synaptic input alter the way the amplitude and time-course of the synaptic input are perceived elsewhere in the tree. As mentioned in footnote 10, the results of this kind of detailed analysis will be given in a forthcoming article.

DISCUSSION

In the preceding sections we have presented an analytical method for ascertaining the time variation in the transmembrane voltage at one point in a branched neuron due to the injection of a time varying current at some other location. Specifically, we extended the treatment developed in Horwitz (1981 *a*) to neurons whose branch diameters are unequal to one another. Several examples were given, along with numerical illustrations. In this remaining section I want to summarize the key points, and to comment on a number of issues to which this work relates.

Comments on the Assumptions Used

The assumptions used in this paper, excluding those concerned with dendritic branch diameters, are the same as in Horwitz (1981 *a*). Most of these are the standard suppositions used in cable theory (Jack et. al., 1975; Rall, 1977); the reader is referred to Horwitz (1981 *a*) and the references cited therein, for a full discussion. However, several points are worth reiterating here. The first, and perhaps the most important, can be subsumed under the heading of linearity. The passive cable properties used in our model imply that the systems we study behave linearly in the following sense: the voltage change due to more than one input is the sum (at any specific time) of the spatially attenuated voltage changes produced by each of the individual inputs. Two kinds of nonlinearities are thus ignored: (*a*) the nonlinear interaction between neighboring synapses due to changes in the driving potentials for synaptic current (e.g., Rall, 1964, 1967, 1970; Rinzel and Rall, 1974; Barrett and Crill, 1974 *b*); (*b*) voltage-dependent cable parameters, which would give rise to spike potentials (e.g., Llinas and Nicholson, 1971).

A point which has been underscored by, among others, Poggio and Reichardt (1980) is that every nontrivial computation performed by the nervous system must be nonlinear. As was illustrated when we compared the graphs of Figs. 8 *A*, 9 *A*, and 9 *B* (see footnote 13), our model is *not* linear in the geometrical parameters. Hence,

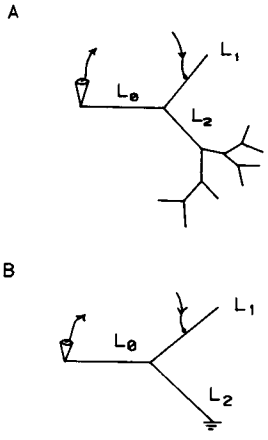

FIGURE 10 (*A*) A dendritic tree in which the synapse lies on the branch of length L_1 is shown. The voltage is to be found at $x = 0$ on the branch of length L_0. There is an elaborate branching pattern past L_2. (*B*) An approximation to the tree shown in *A* is the tree exhibited here. Although L_0 and L_1 have sealed end terminations, we represent the arborization past L_2 by assuming L_2 has a killed-end termination (indicated by the symbol for ground).

[13]Note from Table I that the percentage change corresponding to $f_1 = 1$, $f_2 = x$ ($x = 0.8, 0.63, 0.5$) plus that corresponding to $f_1 = x, f_2 = 1$ almost, but not exactly, equals the percentage change associated with $f_1 = f_2 = x$. The percentage changes will not add because $v(0, t)$ is not linear in the deviations in the branch diameters from equality. However, they almost add because the first-order corrections (which are approximately linear in the deviations) dominate the percentage changes.

two classes of nonlinear computational changes must be distinguished. A change in one or more inputs to a many-input neuron modifies what is computed by that neuron (i.e., its output). A change in the geometrical structure of the neuron, due to development, aging, learning, or pathology, alters how each input contributes to the computation. It is the latter that has been the focus of this article.

The calculations performed in the previous section assumed sealed end boundary conditions at all branch terminations. As discussed in Horwitz (1981 *a*), other boundary conditions (e.g., killed end, lumped soma) can be used. Indeed, in the same neuron some branch terminations can be of one type while others can be of a different type. If some (or all) of the boundary conditions are of the killed end variety, the method developed in this paper can be used to find the correction terms; no complications are encountered. To illustrate, consider the tree shown in Fig. 1 *B* (or Fig. 10 *B*); take the ends of the branches of lengths L_0 and L_1 to be sealed; take the branch of length L_2 to have a killed end; finally, take the synapse to lie on the branch of length L_1. This configuration can represent a neuron in which an injury has occurred. It is also a reasonable model for a dendritic tree in which there is an elaborate branching pattern at the end of L_2 (e.g., Fig. 10 *A*). In this latter case the details of the tree past L_2 are not of interest, but its presence does allow current to be drawn off from the part of the neuron that concerns us.

The expression for $F(\text{Geom}, s)$ is given by Eq. 92 of Horwitz (1981 *a*):

$$F(\text{Geom}, s) = \frac{Z_{c_1} Z_{c_2} \cosh \gamma_1 L_1 \sinh \gamma_2 L_2}{\begin{bmatrix} Z_{c_0} Z_{c_1} \cosh \gamma_0 L_0 \cosh \gamma_1 L_1 \cosh \gamma_2 L_2 \\ + Z_{c_0} Z_{c_2} \cosh \gamma_0 L_0 \sinh \gamma_1 L_1 \sinh \gamma_2 L_2 \\ + Z_{c_1} Z_{c_2} \sinh \gamma_0 L_0 \cosh \gamma_1 L_1 \sinh \gamma_2 L_2 \end{bmatrix}}. \quad (91)$$

We will take $L_0 = L_1 = L_2 \equiv L$. In Horwitz (1981 *a*) we found, when all diameters are equal,[14]

$$f_0(\text{Geom}, t) = \tfrac{1}{4}\,[G_{1i/\sqrt{2};c}(0, t) + G_{1-i/\sqrt{2};c}(0, t)]. \quad (92)$$

If we again let $d_i = f_i d_0$ ($i = 1, 2$), and define $\alpha_{12} = (2 - f_1 - f_2)/2$, then we find for the first-order correction

$$F_0' = -\frac{1}{2d_0}\left[\frac{\sinh \gamma L}{\cosh^2 \gamma L + 2 \sinh^2 \gamma L}\right] \cdot \left[\frac{\gamma L}{\sinh \gamma L \cosh \gamma L\,(\cosh^2 \gamma L + 2 \sinh^2 \gamma L)} + \frac{3\,(\sinh^2 \gamma L + \cosh^2 \gamma L)}{\cosh^2 \gamma L + 2 \sinh^2 \gamma L}\right] \quad (93)$$

which yields (using Eq. 70)

$$f(\text{Geom}, t) = f_0(\text{Geom}, t) * \left(\delta(t) + \frac{\alpha_{12}}{4}\{L[G^{(0)}_{10;c}(L, t) - G^{(0)}_{01;s}(L, t)] * G^{(1)}_{1i/\sqrt{2};c}(0, t) * G^{(0)}_{1-i/\sqrt{2};c}(0, t) + 3 \cdot [G^{(0)}_{1i/\sqrt{2};s}(L, t) + i\,G^{(0)}_{1i/\sqrt{2};c}(L, t)] * [G^{(0)}_{1-i/\sqrt{2};s}(L, t) - i\,G^{(0)}_{1-i/\sqrt{2};c}(L, t)]\}\right) + 0(\alpha_{12}^2). \quad (94)$$

One more point is worth mentioning. All the numerical results in Horwitz (1981 *a*) and in the previous section took the primary branch to be one space constant in length. This was an arbitrary choice; the lengths of the branches are parameters that can be set to values chosen by the person using the model.

Comments on the Correction Terms

Two examples were given to illustrate the theoretical method. Both referred to the tree shown in Fig. 1 *B*. In the first, when the synapse was located on a secondary branch, the approximation techniques needed to obtain the correction terms to the primitive integrals for $v(0, t)$ were applied to the factor $F(\text{Geom}, s)$. In the second, for which the synapse was situated on the primary branch, they were applied to the factor $A(D, s)$. In general, both $F(\text{Geom}, s)$ and $A(D, s)$ must be treated. As stated in Horwitz (1981 *a*), writing the Laplace transformed potential as the product $R(x, s)A(D, s)F(\text{Geom}, s)I_{sy}(s)$ is merely a convenience; it allows a more systematic study of many geometries to be made. Given, then, that the recording location remains at $x = 0$, the approximation techniques must be applied to the product $A(D, s)F(\text{Geom}, s)$. To illustrate, consider the geometry of Fig. 1 *c*. The rules of Butz and Cowan (1974) gives us $V(0, s)$ for the case when the synapse is located on the branch of length L_1:[15]

$$V(0, s) = \frac{Z_{c_0} Z_{c_1} Z_{c_2} \cosh \gamma_2 L_2 \Delta_4}{\Delta_2} I_{sy}(s) \quad (95)$$

where

$$\Delta_4 = Z_{c_1} Z_{c_3} \sinh \gamma_1 (L_1 - D) \cosh \gamma_3 L_3 \sinh \gamma_4 L_4 + Z_{c_1} Z_{c_4} \sinh \gamma_1 (L_1 - D) \sinh \gamma_3 L_3 \cosh \gamma_4 L_4 + Z_{c_3} Z_{c_4} \cosh \gamma_1 (L_1 - D) \cosh \gamma_3 L_3 \cosh \gamma_4 L_4 \quad (96)$$

and

$$\Delta_2 = Z_{c_1} \Delta_a (Z_{c_3} \cosh \gamma_3 L_3 \sinh \gamma_4 L_4 + Z_{c_4} \sinh \gamma_3 L_3 \cosh \gamma_4 L_4) + \Delta_b (Z_{c_3} Z_{c_4} \cosh \gamma_3 L_3 \cosh \gamma_4 L_4) \quad (97)$$

[14]There was a typographical error in the expression for $f(\text{Geom}, t)$ in Horwitz (1981 *a*). Eq. 92 above is the correct result, and it replaces Eq. 94 of Horwitz (1981 *a*).

[15]Note that the version of Eq. 95 used in Appendix A of Horwitz (1981 *a*) contains an error; see footnote 4 for details.

with

$$\Delta_a = Z_{c_0}Z_{c_1}\cosh\gamma_0L_0\sinh\gamma_1L_1\sinh\gamma_2L_2 + Z_{c_0}Z_{c_2}\cosh\gamma_0L_0\cosh\gamma_1L_1\cosh\gamma_2L_2 + Z_{c_1}Z_{c_2}\sinh\gamma_0L_0\sinh\gamma_1L_1\cosh\gamma_2L_2 \quad (98)$$

$$\Delta_b = Z_{c_0}Z_{c_1}\sinh\gamma_0L_0\cosh\gamma_1L_1\cosh\gamma_2L_2 + Z_{c_0}Z_{c_2}\sinh\gamma_0L_0\sinh\gamma_1L_1\sinh\gamma_2L_2 + Z_{c_1}Z_{c_2}\cosh\gamma_0L_0\cosh\gamma_1L_1\sinh\gamma_2L_2. \quad (99)$$

Choosing $R(0, s) = Z_{c_0}$ gives us

$$S(s) \equiv A(D, s)\,F(\text{Geom}, s) = \frac{\cosh\gamma_2L_2\Delta_4}{\Delta_2}. \quad (100)$$

The Taylor expansion is thus performed on $S(s)$:

$$S(s) = S_0 - \alpha_1 d_0(S_1)_0 - \alpha_2 d_0(S_2)_0 + (\alpha_i^2). \quad (101)$$

The procedure by which one evaluates $(S_i)_0$, $(S_{ij})_0$, etc., whether to deal with $A(D, s)$ and $F(\text{Geom}, s)$ separately, or to treat $S(s)$ as a single quantity, depends on the details of the problem. As with any perturbation approach, one must be careful to keep all the terms that contribute to a given order of approximation.

One further point is worth noting. Looking at equations such as 96–100 one sees that it is a rather formidable task to obtain the analytical expressions for $(S_i)_0$, $(S_{ij})_0$, etc. It is formidable in the sense of involving a great deal of algebra (one has to evaluate the derivatives, then set $d_1 = d_2 = \ldots = d_0$). Fortunately, there now exist symbol manipulation programs that can be used to decrease the amount of mental labor. For example, the program REDUCE 2 (Hearn, 1973) was used to check the calculations leading to Eqs. 73, 74, 85, and 86. The crucial point is that the existence of such computer techniques allows higher-order correction terms to be used, if necessary, and it permits us to confront more complicated (and hence, more realistic) geometries.

Comments on the Dependence of the Voltage on Geometry

The trees whose behavior was illustrated in Figs. 8 and 9 are quite simple. Nevertheless, the results of these calculations reinforce the kinds of conclusions that were drawn in our previous studies (Horwitz, 1981 *a*, *b*). Principally, the way in which a synapse is perceived at a given point depends on the geometry of the tree. All the PSPs shown in Figs. 8 *A*, 9 *A*, and 9 *B* correspond to trees in which the physical distance between the input and recording points is the same (this distance equals $L + D$). Yet, as can be seen, the transient voltages recorded at $x = 0$ have quite different rise times, amplitudes and half-widths. Indeed, for the graphs shown in Fig. 9 *A* the electrotonic distance (cf. Rall, 1977) is also the same for each configuration.[16] Therefore, as demonstrated previously by Rall (1967),[17] an evaluation of the shape parameters of the transient voltage response does not allow an unequivocal determination of the physical distance from the soma to the synaptic site, nor does it permit a determination of the electrotonic distance.

The following point can be drawn from this observation: The concept of electrotonic distance, while more useful for a functional analysis than physical distance between input and output sites, is not the measure of synaptic efficacy that provides a reliable way to distinguish different synapses. One value of the use of the model systems introduced here is that they will allow a theoretical search to be made for an appropriate measure of synaptic efficacy, a measure which does not possess the lack of uniqueness seen in the above discussion of electrotonic distance.

Another important conclusion that follows from our analysis was briefly mentioned in footnote 13. The geometrical parameters, the lengths and diameters of the dendritic branches, enter the expression for $v(0, t)$ in a nonlinear way. By being able to evaluate the primitive integrals exactly, as was shown in Horwitz (1981 *a*), and by using a Taylor series to calculate the correction terms, as was shown here, and having found that the first-order percentage changes dominate the corrections, I have managed to develop a method such that the way in which the geometrical parameters affect $v(0, t)$ can be treated (approximately) linearly. In other words, I conjecture that the primitive integral expressions provides the main contribution to the effect of the geometrical pattern of the tree on a PSP; small changes in geometry from the symmetrical tree contribute linearly as far as the major behavior is concerned.

Taper is worth mentioning. We have assumed that each branch is a perfect cylinder. However, real neurons often have dendrites that taper (or sometimes flare). Rall and his colleagues (Rall, 1962 *a*; Goldstein and Rall, 1974), and others (Strain and Brockman, 1975) have shown how, for a single cable, taper may be taken into account. I feel that the method I have developed can give good results and eliminates worry over tapering branches. Taper is important if one has to collapse an entire tree into an equivalent cylinder. The reason this is so is because the 3/2 rule appears less likely to hold in the more distal regions of a

[16]The electrotonic distance is equal to $(L + D)/\lambda_0$, because the branch on on which the synapse is located has the same diameter (and hence the same space constant) as does the primary branch.

[17]Rall (1967) showed, using a compartmental model in which the entire dendritic tree had been replaced by an equivalent cylinder, that one could not infer the location and time course of a synaptic input from the shape of the PSP alone. A given PSP shape could be duplicated by different combinations of input location and synaptic time course. In our study we have found, holding the synaptic time course and location constant, varying the geometry of the tree varies the shapes of the PSP.

dendritic tree (Barrett and Crill, 1974 *a*), and thus the equivalent cylinder method must deal with this by imposing a taper on the cylinder. Our method, working as it does with several branches, can afford to ignore taper, inasmuch as tapering on one or two branches probably will not have a major effect on the behavior of the tree. However, we could handle taper in an approximate way by breaking a single cable into two or more cables in series, each with a different diameter (see Fig. 11 *A*). This can be done by assuming the dendrite bifurcates, but letting one of the lengths go to zero in the Butz-Cowan expression (see Fig. 11 *B*).

Comments on This Method versus Compartmental Models

A model tries to answer a fairly precise set of questions. Thus, it is the questions that determine which model one uses. Many of the efforts of the past have been concerned with using models to aid in extracting values for neuronal parameters from experimental data (e.g., Rall et al., 1967; Jack and Redman, 1971 *a*, *b*; Iansek and Redman, 1973 *a*, *b*; Barrett and Crill, 1974 *a*, *b*). For these kinds of studies the emphasis is on numerical values for the computed potentials. Although some studies treat neuronal morphologies rather exactly (e.g., Turner and Calvin, 1981), many others are content to collapse the dendritic tree into an equivalent cylinder and handle the resulting configuration with a compartmental model (e.g., Rall et al., 1967; Perkel and Mulloney, 1978; Carlen and Durand, 1981). A few analyses presented their computed results in terms of analytical equations (e.g., Rall and Rinzel, 1973; Rinzel and Rall, 1974; Jack and Redman, 1971 *a*, *b*; Redman, 1973). Most of these studies, nevertheless, were ultimately concerned with comparison of computed results with data from specific experimentally analyzed neurons.

The questions I wish to address are different, although they are still derived from experiment. Much evidence had accumulated that connects changes in dendritic morphology with learning, development, aging, and a number of pathologies. These observations have led me, therefore, to attempt to devise a model, as analytical as possible, that will enable me to determine how changes in geometry modify the way electrical information is processed. Although I think that the method I have developed in Horwitz (1981 *a*) and extended here can be used to extract neuronal parameters (it would be especially useful for studying local circuit behavior, where the geometry of part of the dendritic tree must be treated carefully, although some simplifying could take place in other portions of the tree), I am not proposing that my method replace the numerical-compartmental techniques. Rather, I suggest that all these models are complementary, and thus one needs to use the most appropriate model, and that will be the one that allows the specific questions of interest to be addressed.

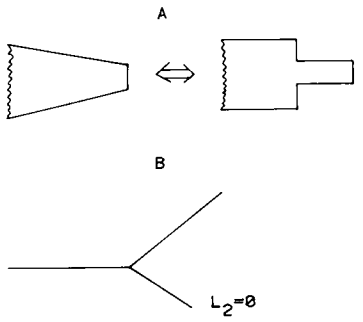

FIGURE 11 (*A*) A way to treat a cable that tapers: represent the tapering cable by two or more constant diameter cables in series. (*B*) The Butz-Cowan formalism deals with the geometry on the right of *A* by using the bifurcating tree shown here and letting L_2 go to zero.

Comments on the Importance of Dendritic Morphology

Obviously this is not the place to review all the experimental studies in which changes in dendritic geometry have been associated with changes in biological activity, but I would like to refer to a few examples to illustrate some key points.

It has become increasingly apparent that the geometry of the dendritic trees of neurons are continually modified during development and aging (e.g., Connor et al., 1981; Buell and Coleman, 1981; Purpura, 1975). The rate at which these changes occur, as well as their functional significance for the animal, can vary dramatically; during early development they are most rapid (Jacobson, 1978), and there are certain critical periods of time when a particluar kind of connection (or stabalization of connections) must be made (e.g., the critical period for the development of binocular vision, see Hubel and Wiesel, 1970). A number of investigators have suggested that the anatomical correlates of long term memory are associated with these same processes (Pribram, 1971; Greenough, 1976; Horwitz, 1981 *b*). Similarly, aberrant morphological changes are linked with pathological conditions. In senile dementia, for example, neurons in some brain regions show greatly reduced dendritic arborizations (Mehraein et al., 1975; Buell and Coleman, 1981). Likewise, it has been shown in an animal model of phenylketonuria that significant alterations in the dendritic branching pattern of motor cortex neurons occur (Hogan and Coleman, 1981).

All of this points to a picture of the dendritic tree as a system in flux. To most investigators this structural plasticity becomes transformed into a functional plasticity by permitting new connections between neurons to be made. This is certainly true. But as can be seen from the examples we presented earlier, and as was stressed in Horwitz (1981 *b*), changes in the geometry of the dendritic tree also affect how previously established synapses are perceived (see also Rall, 1962 *b*). Of course, the strength of a synapse itself can vary, as is observed in such phenomena as

posttetanic potentiation (Bliss and Lomo, 1973). Therefore, as the dendritic tree of a neuron has its geometry modified, new synapses can form (and old ones can disengage), the way previously existing synapses are perceived changes (as alternative current pathways become available), and finally, by a variety of mechanisms, the actual strength of a synapse can vary. All three modes contribute to an alteration in the neuronal computation. The analytical model outlined here allows an assessment of the consequences of these kinds of neuronal plasticity to be made in a systematic and quantitative manner.

An important problem emerges once we recognize that synaptic efficacy depends on dendritic architecture. This problem is the inverse of neuronal plasticity. Some connections, once made, should always be perceived in the same way. Thus, there is a need for mechanisms to maintain a specific response in the face of anatomical change. There are a large number of possibilities. For example, the strength of a given synapse might be adjusted to compensate for dendritic growth distal to the synapse. Alternatively, dendritic growth in one region of a tree may influence growth elsewhere in such a way as to maintain synaptic invariance. This may account for the observation of Glasser (1977) who looked at the morphology of the same identifiable neuron from seven different individual lobsters. Although the number and diameters of major branches differed by 20–30%, as did the conductances of defined substructures, when voltage decrement curves were calculated by means of a computer model, she found that the curves resembled one another to within 10%. Thus, the seven cells would behave similarly; differences in physical structure and differences in electrical parameters were found to produce uniformity in electrotonic (and presumably functional) behavior. Generalizing, we might conjecture that there exist a set of "equivalent trees" such that a given synapse would be perceived in the same way in all members of the set. Our analytical method would allow a search for such sets to be made. Indeed, such an effort is currently under way.

Concluding Comments

It now seems clear that understanding local circuit behavior is central to understanding neural functioning (Schmitt et al., 1976; Rakic, 1976; Shepherd, 1979). This means that the electrotonic properties of neurons must be studied, and that the complex geometry of dendritic trees must be realistically included. The method I have developed offers an approach to these difficult problems. By having an analytical treatment, a systematic, quantitative analysis of how changes in geometry affect PSP spread can be made. Of course, to talk about anything one needs a language. The G-function formalism gives us the "words" for this language. They allow for a precise description of the structure-function relationship of neuronal dendritic trees.

I wish to thank Sue Wunschel and Rebecca Bonney for assistance.

This research was supported in part by institutional research grants from Texas Woman's University.

Received for publication 2 March 1982 and in revised form 7 July 1982.

REFERENCES

Barrett, J. N., and W. E. Crill. 1974 *a*. Specific membrane properties of cat motoneurones. *J. Physiol. (Lond.)*. 239:301–324.

Barrett, J. N., and W. E. Crill. 1974 *b*. The influence of dendritic location and membrane properties on the effectiveness of synapses on cat motoneurones. *J. Physiol. (Lond.)*. 239:325–345.

Bliss, T. V. P., and T. Lomo. 1973. Long-lasting potentiation of synaptic transmission in the dentate area of the anaesthetized rabbit following stimulation of the perforant path. *J. Physiol. (Lond.)*. 232:331–356.

Buell, S. J., and P. D. Coleman. 1981. Quantitative evidence for selective dendritic growth in normal human aging but not in senile dementia. *Brain Res.* 214:23–41.

Butz, E. G., and J. D. Cowan. 1974. Transient potentials in dendritic systems of arbitrary geometry. *Biophys. J.* 14:661–689.

Carlen, P. L., and D. Durand. 1981. Modeling the postsynaptic location and magnitude of tonic conductance changes resulting from neurotransmitters or drugs. *Neuroscience.* 6:839–846.

Churchill, R. V. 1958. Operational Mathematics. McGraw-Hill, Inc., New York.

Connor, J. R., M. C. Diamond, J. A. Connor, and R. E. Johnson. 1981. A Golgi study of dendritic morphology in the occipital cortex of socially reared aged rats. *Exp. Neurol.* 73:525–533.

Glasser, S. 1977. Computer reconstruction and passive modeling of identified nerve cells in the lobster stomatogastric ganglion. Ph.D Dissertation. University of California, San Diego, CA.

Goldstein, S. S., and W. Rall. 1974. Changes of action potential shape and velocity for changing core conductor geometry. *Biophys. J.* 14:731–757.

Greenough, W. T. 1976. Enduring brain effects of differential experience and training. *In* Neural Mechanisms of Learning and Memory. M. R. Rosenzweig and E. L. Bennett, editors. MIT Press, Cambridge, Mass. 255–278.

Hearn, A. C. 1973. REDUCE 2, A system and language for algebraic manipulation. *In* Proceedings of the Second Symposium on Symbolic and Algebraic Manipulation.

Hogan, R. N., and P. D. Coleman. 1981. Experimental hyperphenylalaninemia:o dendritic alterations in motor cortex of rat. *Exp. Neurol.* 74:218–233.

Horwitz, B. 1981 *a*. An analytical method for investigating transient potentials in neurons with branching dendritic trees. *Biophys. J.* 36:155–192.

Horwitz, B. 1981 *b*. Neuronal plasticity: how changes in dendritic architecture can affect the spread of postsynaptic potentials. *Brain Res.* 224:412–418. (See erratum, 238:505 [1982].)

Horwitz, B. 1981 *c*. Beyond the 3/2 rule: Unequal lengths and diameters and their effects on transient voltages in neurons with branching dendritic trees. *Soc. Neurosci. Abstr.* 7:360.

Hubel, D. H., and T. N. Wiesel. 1970. The period of susceptibility to the physiological effects of unilateral eye closure in kittens. *J. Physiol. (Lond.)*. 206:419–436.

Iansek, R., and S. J. Redman. 1973 *a*. An analysis of the cable properties of spinal motoneurones using a brief intracellular current pulse. *J. Physiol. (Lond.)*. 234:613–636.

Iansek, R., and S. J. Redman. 1973 *b*. The amplitude, time course and charge of unitary post-synaptic potentials evoked in spinal motoneurone dendrites. *J. Physiol. (Lond.)*. 234:665–688.

Jack, J. J. B., D. Noble, and R. W. Tsien. 1975. Electric Current Flow in Excitable Cells. Oxford University Press, Oxford.

Jack, J. J. B., and S. J. Redman. 1971 *a*. The propagation of transient potentials in some linear cable structures. *J. Physiol. (Lond.)*. 215:283–320.

Jack, J. J. B., and S. J. Redman. 1971 *b*. An electrical description of the motoneuron, and its application to the analysis of synaptic potentials. *J. Physiol.* (*Lond.*). 215:321–352.

Jacobson, M. 1978. Developmental Neurobiology. 2nd Edition. Plenum Publishing Corp., New York.

Llinas, R., and C. Nicholson. 1971. Electrophysiological properties of dendrites and somata in alligator Purkinje cell. *J. Neurophysiol.* (*Bethesda*). 34:532–551.

Magnus, W., F. Oberhettinger, and R. P. Soni. 1966. Formulas and Theorems for the Special Functions of Mathematical Physics. Springer-Verlag New York, Inc., New York. 323–327.

Mehraein, P., M. Yamada, and E. Tarnowska–Dziduszko. 1975. Quantitative study on dendrites and dendritic spines in Alzheimer's disease and senile dementia. *Adv. Neurol.* 12:453–458.

Oberhettinger, F., and L. Badii. 1973. Tables of Laplace Transforms. Springer-Verlag New York, Inc., New York. 259.

Perkel, D. H., and B. Mulloney. 1978. Electrotonic properties of neurons: Steady-state compartmental model. *J. Neurophysiol.* (*Bethesda*). 41:621–639.

Poggio, T., and W. Reichardt. 1980. On the representation of multi-input systems: computational properties of polynomial algorithms. *Biol. Cybern.* 37:167–186.

Pribram, K. H. 1971. Languages of the Brain: Experimental Paradoxes and Principles in Neuropsychology. Prentice-Hall, Inc., Englewood Cliffs, New Jersey. 26–47.

Purpura, D. P. 1975. Dendritic differentiation in human cerebral cortex: normal and aberrant developmental patterns. *Adv. Neurol.* 12:91–116.

Rakic, P., Editor. 1976. Local Circuit Neurons. MIT Press, Cambridge, Mass.

Rall, W. 1962 *a*. Theory of physiological properties of dendrites. *Ann. N. Y. Acad. Sci.* 96:1071–1092.

Rall, W. 1962 *b*. Electrophysiology of a dendritic neuron model. *Biophys. J.* (*Suppl.*). 2(2, part 2):145–167.

Rall, W. 1964. Theoretical significance of dendritic trees for neuronal input-output relations. *In* Neural Theory and Modeling. R. F. Reiss, editor. Stanford University Press, Stanford, CA. 73–97.

Rall, W. 1967. Distinguishing theoretical synaptic potentials computed for different soma-dendritic distributions of synaptic input. *J. Neurophysiol.* (*Bethesda*). 30:1138–1168.

Rall, W. 1970. Cable properties of dendrites and effects of synaptic location. *In* Excitatory Synaptic Mechanisms. P. Andersen and J. K. S. Jansen, editors. Universitetsforlaget, Oslo. 175–187.

Rall, W. 1977. Core conductor theory and cable properties of neurons. *In* Handbook of Physiology (Sect. 1) The Nervous System. I. Cellular Biology of Neurons. E. R. Kandel, editor. Am. Physiol. Soc., Bethesda, MD. 39–97.

Rall, W., R. E. Burke, T. G. Smith, and K. Frank. 1967. Dendritic location of synapses and possible mechanisms for the monosynaptic EPSP in motoneurons. *J. Neurophysiol.* (*Bethesda*). 30:1169–1193.

Rall, W., and J. Rinzel. 1973. Branch input resistance and steady attenuation for input to one branch of a dendritic neuron model. *Biophys. J.* 13:648–688.

Redman, S. J. 1973. The attenuation of passively propagating dendritic potentials in a motoneurone cable model. *J. Physiol.* (*Lond.*). 234:637–664.

Rinzel, J., and W. Rall. 1974. Transient response in a dendritic neuron model for current injected at one branch. *Biophys. J.* 14:759–790.

Schmitt, F. O., P. Dev, and B. H. Smith. 1976. Electrotonic processing of information by brain cells. *Science* (*Wash., D. C.*). 193:114–120.

Shepherd, G. M. 1979. The Synaptic Organization of the Brain. 2nd Edition. Oxford University Press, Oxford.

Strain, G. M., and W. H. Brockman. 1975. A modified cable model for neuron processes with non-constant diameters. *J. Theor. Biol.* 51:475–494.

Turner, D. A., and W. H. Calvin. 1981. Dendritic analysis of lobster stretch receptor neurons: electrotonic properties with single and distributed inputs. *Cell. Mol. Neurobiol.* 1:189–207.